Three Dimensional Digital Polyhedral Phantom Framework with Analytical Fourier Transform and Application in Cardiac Imaging

T. M. Ngo[1], G. S. Fung[2], B. M. Tsui[1,2], E. McVeigh[1], and D. A. Herzka[1]
[1]Department of Biomedical Engineering, Johns Hopkins School of Medicine, Baltimore, Maryland, United States, [2]Division of Medical Imaging Physics, Department of Radiology, Johns Hopkins School of Medicine, Baltimore, Maryland, United States

Introduction: Physiologically relevant computer simulations involving digital phantoms are commonly used to test new MR acquisition and reconstruction strategies in cases where real experiments are unfeasible or impractical. Although these phantoms are constructed in the image domain, since MR samples Fourier space, these phantoms must also provide an accurate Continuous Fourier Transform (CFT) representation. However, computing the CFT at any arbitrary point in k-space from an image domain description of a phantom can be difficult. Voxel-based phantoms approximate the CFT by computing the Discrete Fourier Transform (DFT) of a super-sampled image of the phantom. This approach is both computationally inefficient and not directly applicable when non-Cartesian k-space sampling patterns are desired. Alternatively, analytical phantoms are constructed using geometric primitives such as ellipsoids, whose CFT are known analytically [1]. To date, this approach has been limited because these primitives are unable to model complicated anatomical shapes. Here, we extend this approach and present a framework that allows realistic 3-D digital phantoms to be created from general polyhedra which also have an analytical CFT solution. Polyhedra are closed surfaces comprised of polygonal faces and include standard triangular meshes widely used in 3-D computer modeling. We demonstrate the value of the framework with a simple experiment in which we created a realistic MR heart phantom derived from the 4-D eXtended CArdiac Torso (XCAT) phantom and simulated motion artifacts which arise during segmented, cardiac gated cine acquisitions.

Methods: Komrska [2] derives the analytical solution for the Fourier transform $S(\boldsymbol{k})$ of a constant unitary valued polyhedral solid at position $\boldsymbol{k}$ as:

$$S(\boldsymbol{k}) = \begin{cases} -\frac{1}{(2\pi k)^2}\sum_{f=1}^{F} S_f^*(\boldsymbol{k}), & \boldsymbol{k} \neq \boldsymbol{0} \\ V, & \boldsymbol{k} = \boldsymbol{0} \end{cases} \qquad S_f^*(\boldsymbol{k}) = \begin{cases} \frac{\boldsymbol{k}\cdot\widehat{\boldsymbol{N}}_f}{k^2-(\boldsymbol{k}\cdot\widehat{\boldsymbol{N}}_f)^2}\sum_{e=1}^{E_f} L_{fe}\boldsymbol{k}\cdot\widehat{\boldsymbol{n}}_{fe}\frac{\sin(\pi\boldsymbol{k}\cdot\hat{\boldsymbol{t}}_{fe}L_{fe})}{\pi\boldsymbol{k}\cdot\hat{\boldsymbol{t}}_{fe}L_{fe}}\exp\left(-2\pi i\boldsymbol{k}\cdot\boldsymbol{r}^{(C_{fe})}\right), & \boldsymbol{k} \neq k\widehat{\boldsymbol{N}}_f \\ -2\pi i\boldsymbol{k}\cdot\widehat{\boldsymbol{N}}_f \exp\left(-2\pi i\boldsymbol{k}\cdot\boldsymbol{r}^{(V_{f1})}\right)P_f, & \boldsymbol{k} = k\widehat{\boldsymbol{N}}_f \end{cases}$$

Where V is the volume of the polyhedron and P_f is the area of the f[th] face given respectively as [3]:

$$V = \frac{1}{6}\left|\left[\sum_{f=1}^{F}\left(\boldsymbol{r}^{V_{f1}}\cdot\widehat{\boldsymbol{N}}_f\right)\left|\widehat{\boldsymbol{N}}_f\cdot\left\{\sum_{e=1}^{E_f}\boldsymbol{r}^{(V_{fe})}\times\boldsymbol{r}^{(V_{fe+1})}\right\}\right|\right]\right| \qquad P_f = \frac{1}{2}\sum_{e=1}^{E}\left|\widehat{\boldsymbol{N}}_f\cdot\{\boldsymbol{r}^{(V_{fe})}\times\boldsymbol{r}^{(V_{fe+1})}\}\right|$$

Let F: total faces, $\widehat{\boldsymbol{N}}_f$: unit normal of f[th] face, L_{fe}: length of e[th] edge of f[th] face, E_f: total edges in f[th] face, $\boldsymbol{r}^{(C_{fe})}$: position vector of the midpoint of e[th] edge on f[th] face, $\hat{\boldsymbol{t}}_{fe}$: Unit vector in the direction of e[th] edge of f[th] face, L_{fe}: Length of e[th] edge of f[th] face, $\widehat{\boldsymbol{n}}_{fe}$: outward normal to e[th] edge of f[th] face in the plane of face P_f, $\boldsymbol{r}^{(V_{fe})}$: position vector of e[th] vertex of f[th] face ordered counterclockwise when viewed against $\widehat{\boldsymbol{N}}_f$, k: magnitude of $\boldsymbol{k}$. Edge e on face f points from vertex $\boldsymbol{r}^{(V_{fe})}$ to $\boldsymbol{r}^{(V_{fe+1})}$. Additionally, the first and last vertices are connected, thus $V_{E+1} = V_1$ and likewise $V_0 = V_E$. Fig. 1 illustrates these vectors.

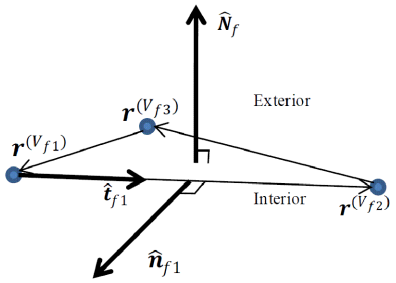

Figure 1: Vectors which define a single face of the 3-D polyhedron.

Implementation: The framework is implemented as a Matlab C++ plug-in, parallelized using the cross platform ITK library. The cost of computing the CFT of the phantom is linear with the number of polygonal faces and k-space samples. The face contributions $S_f^*(\boldsymbol{k})$ can be computed in parallel. A quad core Intel Xeon 2.13Ghz system computes a 51x51x51 matrix, or 132,651 k-space samples for a polyhedron with 1,612 triangular faces in ~110 seconds (3 run average), 0.5136 μseconds/sample/face.

Experiment: Using our framework, we created a realistic phantom of the beating left and right ventricles which were then used to simulate a standard Cartesian segmented, cardiac gated cine acquisition. The XCAT phantom, which derives both geometry and motion from human physiological measurements [4], provided triangular meshes for the polyhedral phantom. 100 evenly spaced snapshots of the left and right ventricle throughout a cardiac cycle were generated from the non-uniform rational B-spline (NURBS) surfaces of the XCAT heart model. Each snapshot provided separate triangular meshes for the endocardial and epicardial surfaces of the left and right ventricles for a total of 13,000 faces per time sample. Fig. 2 illustrates these meshes at systole. We then simulated a 3-D cine segmented Cartesian acquisition with the following parameters: Heart rate: 60 BPM, TR: 3.5 ms, 15/9/5 phase encodes per segment (18/30/48 cardiac phases, 52.5/27/17.5 ms, ~19/37/57 Hz temporal resolution), matrix size 128^3, FOV 100x112x80 mm yielding a physically unachievable resolution of 0.77x0.87x0.625 mm.

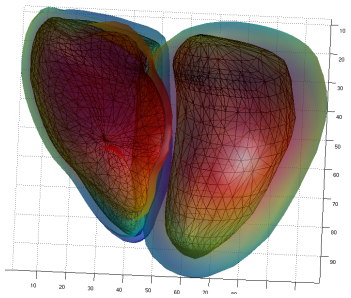

Figure 2: Triangular meshes of left and right ventricles of cardiac phantom at systole. Wireframe: endocardial, translucent: epicardial.

Results: Fig. 3 shows long and short axis slices of the inverse DFT reconstructed volume at cardiac phases corresponding to end systole, shortly after systole, and mid-diastole. As expected, images of the semi-quiescent periods at end-systole and mid-diastole are relatively artifact free, regardless of sampling rate, while those during iso-volumic relaxation exhibit motion artifacts. These artifacts are edge enhanced ghosts similar to those observed during real acquisitions [5]. The white boundary in the septum is caused by correctible overlap between the meshes.

Conclusion: Previously presented analytical phantoms could not represent complex anatomical shapes. Using polyhedra, our framework allows construction of realistic digital phantoms that still have an analytical CFT. This is particularly useful for non-Cartesian acquisition techniques. Though not shown here, the 4D XCAT includes thousands of anatomically correct structures, including the chest wall, larger vasculature, and coronary arteries, and models both cardiac and respiratory motion. Using our framework in conjunction with meshes derived from the XCAT phantom will provide physiologically realistic image and k-space gold standards, thus facilitating the development of acquisition, motion compensation, and reconstruction techniques.

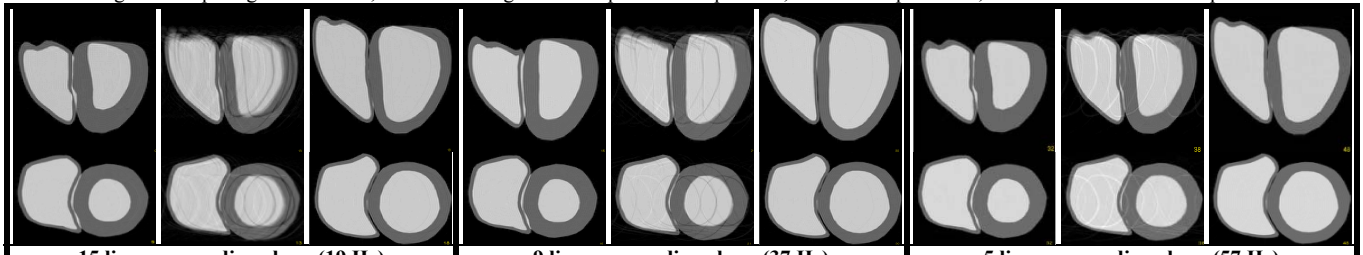

Figure 3: Reconstructed slices of phantom simulation. Top row: long axis, Bottom row: short axis. Columns left to right within a temporal resolution grouping are systole, shortly after systole at the moment with maximum motion artifact and mid-diastole.

[1] C. G. Koay, et al MRM 2007, 58(2):430. [2] J. Komrska, Optik 1988, 80(4): 171. [3] J. Arvo, Graphics Gems II (Graphics Gems - IBM), 1991 Academic Press. [4] WP. Segars et al. Proc. of the IEEE 2009, 97(12):1954-1968. [5] Haacke et al. MRI: Physical Principles and Design, Chap. 23 1999 Wiley-Liss.